IOP Publishing | Royal Swedish Academy of Sciences Physica Scripta
Phys. Scr. 91 (2016) 114001 (9pp) doi:10.1088/0031-8949/91/11/114001

Molecular dynamics and reverse Monte Carlo modeling of scheelite-type AWO_4 (A = Ca, Sr, Ba) W L_3-edge EXAFS spectra

Aleksandr Kalinko[1,2], Matthias Bauer[1], Janis Timoshenko[3] and Alexei Kuzmin[4]

[1] Universität Paderborn, Naturwissenschaftliche Fakultät, Department Chemie, Warburger Straße 100, D-33098 Paderborn, Germany
[2] DESY Photon Science, Notkestrasse 85, D-22607 Hamburg, Germany
[3] Physics Department, Yeshiva University, New York, NY 10016, USA
[4] Institute of Solid State Physics, University of Latvia, Kengaraga street 8, LV-1063 Riga, Latvia

E-mail: aleksandr.kalinko@desy.de

Received 27 June 2016, revised 22 September 2016
Accepted for publication 27 September 2016
Published 18 October 2016

Abstract

Classical molecular dynamics (MD) and reverse Monte Carlo methods coupled with *ab initio* multiple-scattering extended x-ray absorption fine structure (EXAFS) calculations were used for modeling of scheelite-type AWO_4 (A = Ca, Sr, Ba) W L_3-edge EXAFS spectra. The two theoretical approaches are complementary and allowed us to perform analysis of full EXAFS spectra. Both methods reproduce well the structure and dynamics of tungstates in the outer coordination shells, however the classical MD simulations underestimate the W–O bond MSRD due to a neglect of quantum zero-point-motion. The thermal vibration amplitudes, correlation effects and anisotropy of the tungstate structure were also estimated.

Keywords: tungstates, EXAFS, W L_3-edge, molecular dynamics, reverse Monte Carlo

(Some figures may appear in colour only in the online journal)

1. Introduction

Extended x-ray absorption fine structure (EXAFS) is a powerful experimental technique to study local environment of a particular atom in a material [1–3]. However, the accurate analysis of the EXAFS spectra is often limited due to difficulties related to accounting for the multiple-scattering (MS) contributions, structural and thermal disorder effects [4, 5]. These issues are commonly addressed using modern computer codes as FEFF [6, 7], GNXAS [5, 8] or DL_EXCURV [9, 10]. An alternative approach to incorporate disorder effects into the MS formalism is based on molecular dynamics (MD) [11–16] or reverse Monte Carlo (RMC) [17–19] simulations.

The MD approach requires the knowledge of interatomic potentials but gives the trajectories of atoms, which can be used to extract useful information on vibrational properties of the material [20]. The control of the trajectory length allows one also to accumulate sufficiently good statistics required for accurate determination of structural parameters. However, classical MD simulations neglect quantum effects and, thus, will fail in the low-temperature range, resulting in underestimated amplitudes of vibrations. On the contrary, the RMC method deals with a single configuration which is fitted to the experimental data and can be employed equally well at any temperature. In particular, our original realization of the RMC method utilizes evolutionary algorithm (EA) for structure optimization [21], and the wavelet transform of the EXAFS spectrum is used as a criterion of the best agreement between experimental and theoretical EXAFS spectra taking into account their behavior in wavenumber and real spaces simultaneously [22, 23]. The principle difference between the MD and RMC methods from the structural model point of view is that in the former method the model is uniquely defined by the MD simulation, whereas in the latter it is obtained as a result of the fit to the experimental data. Thus, the use of both MD and RMC methods improves the

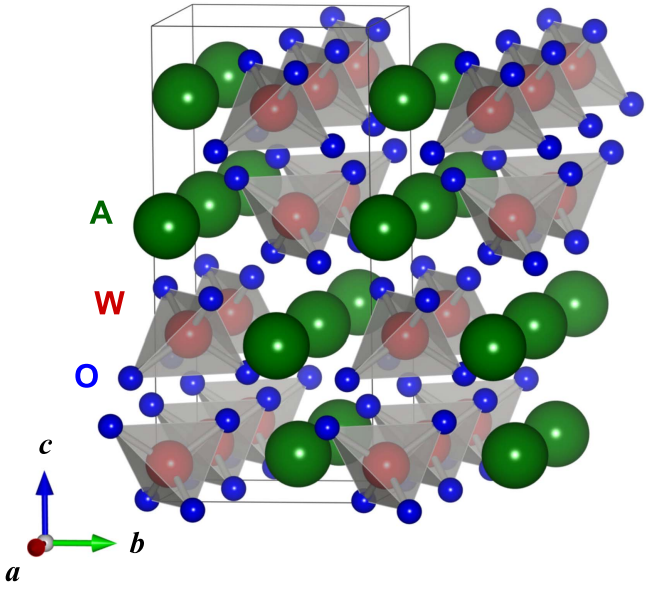

Figure 1. Crystal structure of scheelite-type AWO_4 (A = Ca, Sr, Ba) tungstates [30, 31]. Crystallographic unit cell is indicated.

Table 1. Lattice parameters ($a = b$, c, $\alpha = \beta = \gamma = 90°$) and the values of two internal O–W–O bond angles and two groups of the O–O distances in compressed along c-axis WO_4 tetrahedra for scheelite-type AWO_4 (A = Ca, Sr, Ba) tunsgtates (space group $I4_1/a$ (88), $Z = 4$) [30, 31].

	$CaWO_4$	$SrWO_4$	$BaWO_4$
a, b (Å)	5.244	5.417	5.613
c (Å)	11.376	11.951	12.720
$\widehat{OWO}_1$ (°)	107.25	107.58	108.11
$\widehat{OWO}_2$ (°)	114.01	113.32	112.23
2 × R(O–O) (Å)	3.002	2.972	2.958
4 × R(O–O) (Å)	2.881	2.870	2.885

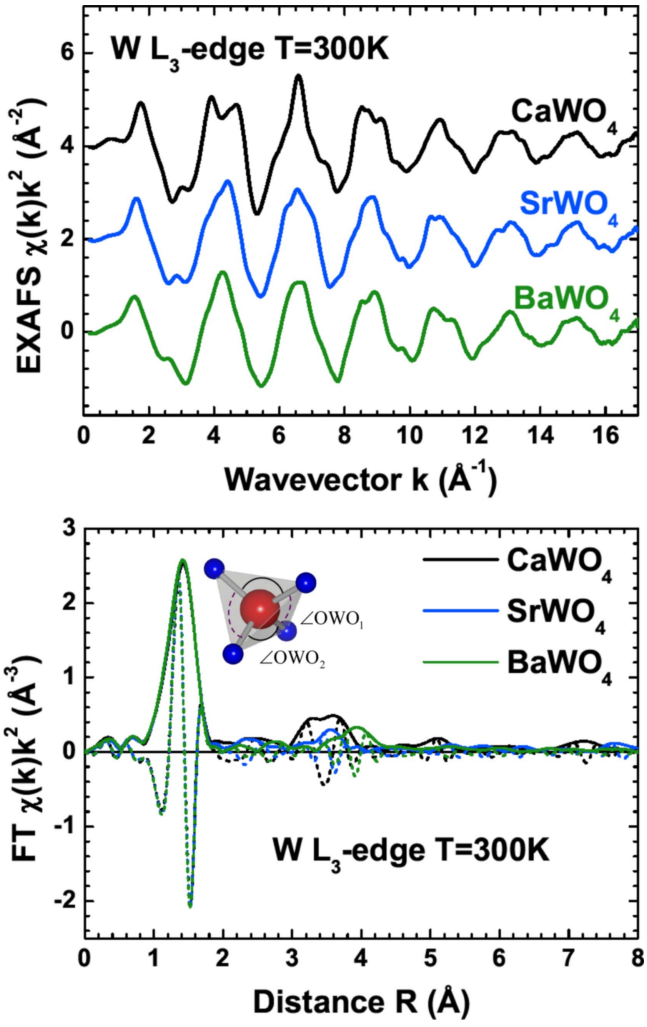

Figure 2. Comparison of the experimental W L_3-edge EXAFS $\chi(k)k^2$ spectra and their Fourier transforms (modulus and imaginary parts are shown) in scheelite-type AWO_4 (A = Ca, Sr, Ba) tungstates at $T = 300$ K. The inset shows distorted WO_4 tetrahedron with four small ($\angle OWO_1$) and two large ($\angle OWO_2$) internal O–W–O bond angles.

reliability of the obtained results. In this study we demonstrate such approach on example of scheelite-type AWO_4 (A = Ca, Sr, Ba) compounds.

Most tungstates with the formula AWO_4 are known to crystallize in scheelite- or wolframite-type structures depending on the size of the bivalent A^{2+} cations [24, 25]. The crystalline structure of wolframites with monoclinic space group $P2/c$ consists of infinite zigzag chains entirely built up of distorted WO_6 and AO_6 octahedra connected by edges. The degree of octahedra distortion, which depends on the type of metal cations and the crystallite size, has been studied by us recently using RMC method [26–29].

Scheelite-type AWO_4 (A = Ca, Sr, Ba) tungstates (figure 1 and table 1) have tetragonal symmetry (space group $I4_1/a$ (88), $Z = 4$) [30, 31]. The W^{6+} and alkaline Earth metal A^{2+} cations are tetrahedrally WO_4 and eightfold AO_8 coordinated to the oxygen atoms. While all W–O bonds are equal (1.789 Å in $CaWO_4$, 1.778 Å in $SrWO_4$, and 1.782 Å in $BaWO_4$), the WO_4 tetrahedra are slightly distorted, being compressed along c-axis, with two long and four short R(O–O) distances. As a result, the tetrahedra have four smaller ($\angle OWO_1$) and two larger ($\angle OWO_2$) internal O–W–O bond angles compared to their values in regular WO_4 tetrahedron (109.47°). While a substitution of alkaline Earth ions affects barely the first coordination shell of tungsten atoms, which can be easily studied using conventional EXAFS analysis [32–35], it is more difficult to follow the changes occurring at distant shells due to a need to account for both MS and thermal disorder effects simultaneously. Therefore, to treat these challenging problems and to extract structural (bond lengths) and dynamical (amplitude of atomic displacements) information from the W L_3-edge EXAFS spectra of AWO_4 tungstates we employ two complementary techniques based on MD and RMC simulations.

2. Experimental

Commercially available polycrystalline AWO_4 powders (A = Ca, Sr, Ba; 99.9% purity) were used in all measurements. The phase purity of the samples was confirmed by

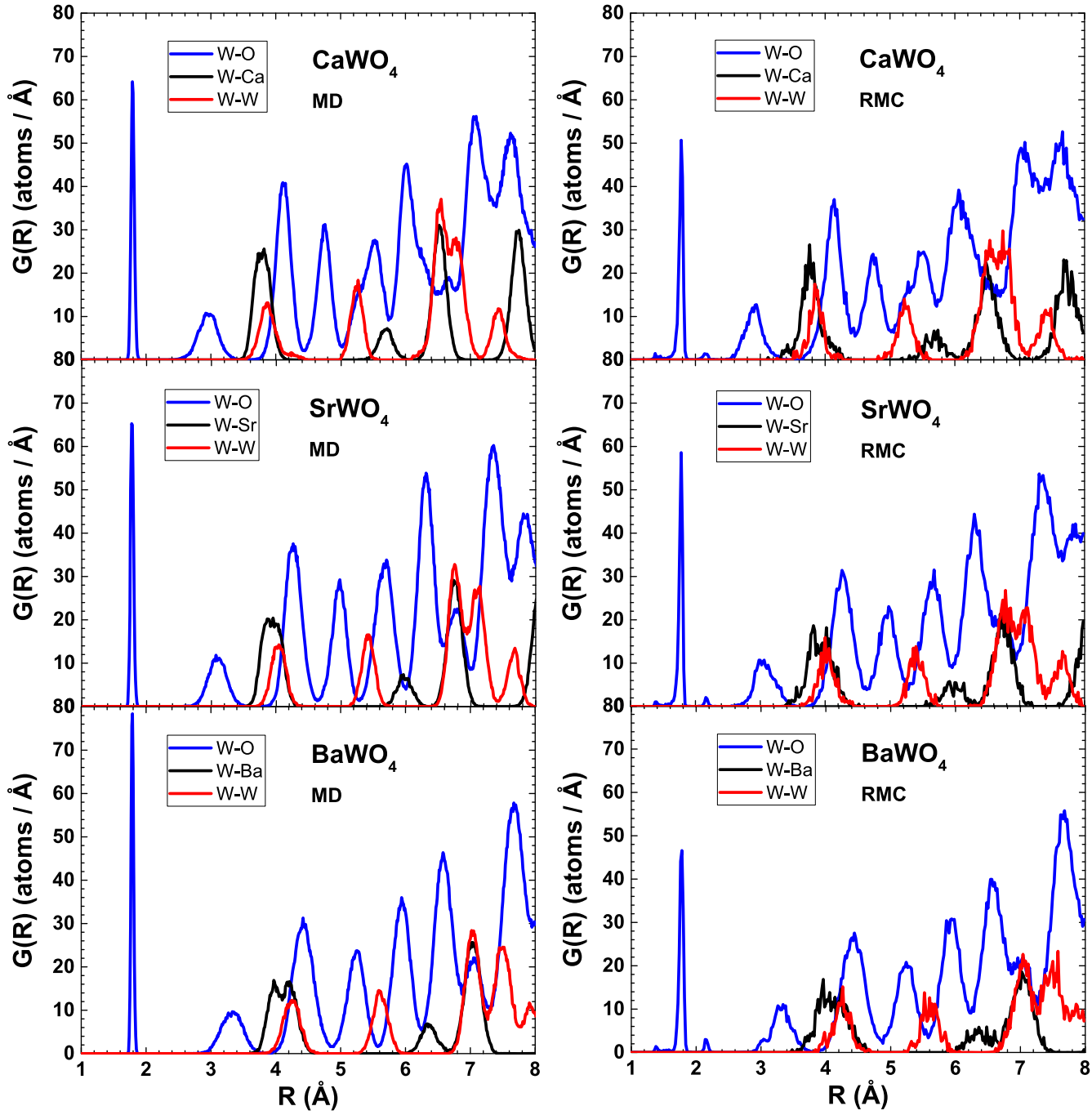

Figure 3. Comparison of the partial radial distribution functions $G(R)$ in scheelite-type AWO_4 (A = Ca, Sr, Ba) tungstates at $T = 300$ K obtained by MD and RMC/EA methods.

x-ray powder diffraction and micro-Raman spectroscopy measurements.

X-ray absorption experiments were performed at the W L_3-edge (10207 eV) in transmission mode at the HASYLAB DESY C1 bending-magnet beamline at $T = 300$ K [36]. The storage ring DORIS III operated at $E = 4.44$ GeV and $I_{max} = 140$ mA. The x-ray beam intensity was measured by two ionization chambers filled with argon gas. The higher order harmonics were effectively eliminated by detuning of the double-crystal monochromator Si(111) to 60% of the rocking curve maximum, using the beam-stabilization feedback control. The powder samples were deposited on Millipore filters and fixed by Scotch tape. The thickness x of the deposited sample was optimized to give the value of the absorption W L_3-edge jump close to $\Delta\mu x \approx 1$.

The experimental W L_3-edge EXAFS spectra $\chi(k)k^2$ were extracted using a conventional procedure [37] implemented in the EDA package [38]. The origin of the photoelectron kinetic energy E_0, used in the definition of the wavenumber $k = \sqrt{(2m_e/\hbar^2)(E - E_0)}$ (m_e is the electron mass, $\hbar$ is the Plank's constant), was chosen to align best the energy scale of the experimental and theoretical EXAFS spectra [3, 37].

The EXAFS spectra for three tungstates are shown together with their Fourier transforms (FTs) in figure 2. Note that all FTs reported here were not corrected for the backscattering phase shift of atoms, therefore the positions of all peaks are displaced to smaller distances relative to their crystallographic values. While the crystallographic structure of these tungstates is close (figure 1 and table 1), the difference between backscattering amplitudes and phases of the A^{2+} cations is responsible for a variation of their EXAFS spectra. The FTs are dominated by the main peak at 1.4 Å, which corresponds to four nearest oxygen atoms forming WO_4 tetrahedron around the absorbing tungsten atom. The A^{2+} cations contribute to the next peak at 3–4 Å.

Table 2. Comparison of the nearest interatomic distances R(W–O) (in Å), mean square displacements (MSD(O) and MSD(W), in Å^2), and mean square relative displacements (MSRD(W–O), in Å^2) obtained from the analysis of the experimental diffraction data [30, 31] with the results of molecular dynamics simulations and reverse Monte Carlo approach based on evolutionary algorithm.

	$CaWO_4$	$SrWO_4$	$BaWO_4$
	Experimental diffraction data		
R_D(W–O)	1.789	1.779	1.781
MSD_D(W)	0.0058, 0.0113	0.0044	0.0083
MSD_D(O)	0.0098, 0.0139	0.0075	0.014
	Molecular dynamics		
R_{MD}(W–O)	1.793	1.775	1.788
MSD_{MD}(W)	0.0065	0.0063	0.0081
MSD_{MD}(O)	0.0093	0.0102	0.0142
$MSRD_{MD}$(W–O)	0.0006	0.0006	0.0004
	RMC/EA		
R_{RMC}(W–O)	1.785	1.784	1.788
MSD_{RMC}(W)	0.0061	0.0085	0.0098
MSD_{RMC}(O)	0.0113	0.0131	0.0133
$MSRD_{RMC}$(W–O)	0.0011	0.0008	0.0010

3. MD simulations

The classical MD simulations were performed in the canonical (NVT) ensemble using the GULP4.2 code [39, 40]. The force-field models of tungstates were reported by us previously [41]. They were constructed as a sum of Coulomb, Buckingham (for A–O and O–O atom pairs), Morse (for W–O atom pair) and three-body harmonic (for O–W–O bonds) potentials. The values of potential parameters were taken for $CaWO_4$ from [42], whereas for $SrWO_4$ and $BaWO_4$ from [41]. The simulation box was a supercell $5a \times 5b \times 4c$ containing 1200 atoms with periodic boundary conditions. The simulation temperature was set to 300 K as in the EXAFS experiment and kept nearly constant during each simulation using the Nosé–Hoover thermostat [43]. The Newton's equations of motion were integrated using the Verlet leapfrog algorithm [44]. A set of 10 000 static atomic configurations was accumulated during each MD run of 50 ps with the time step of 0.5 fs. These configurations (atomic coordinates) were further used to calculate the configuration-averaged W L_3-edge EXAFS spectrum by the MD-EXAFS approach [15, 45] as well as to determine partial radial distribution functions (RDFs) G(W–O), G(W–W), and G(W–A) (figure 3), the

Table 3. Structural parameters (N is the coordination number, R is the interatomic distance (in Å), and σ^2 is the MSRD (in Å^2)) for AWO_4 (A = Ca, Sr, Ba) obtained from a decomposition of the radial distribution functions into a set of Gaussian functions for the first five coordination shells (up to 4.5 Å) of tungsten.

		$CaWO_4$		$SrWO_4$		$BaWO_4$	
	N	R	σ^2	R	σ^2	R	σ^2
				Molecular dynamics			
W–O1	4	1.793	0.0006	1.775	0.0006	1.788	0.0004
W–O2	4	2.961	0.0215	3.094	0.0200	3.327	0.0283
W–A3	4	3.689	0.0052	3.826	0.0076	3.952	0.0088
	4	3.843	0.0093	4.026	0.0095	4.220	0.0140
W–W4	4	3.870	0.0138	4.035	0.0124	4.247	0.0168
W–O5	12	4.120	0.0129	4.262	0.0162	4.422	0.0256
				RMC/EA			
W–O1	4	1.781	0.0008	1.777	0.0006	1.773	0.0009
W–O2	4	2.901	0.0167	3.065	0.0236	3.321	0.0200
W–A3	8	3.771	0.0154	3.922	0.0381		
	4					3.941	0.0142
	4					4.248	0.0217
W–W4	4	3.863	0.0081	4.018	0.0142	4.249	0.0152
W–O5	12	4.131	0.0173	4.267	0.0255	4.424	0.0340

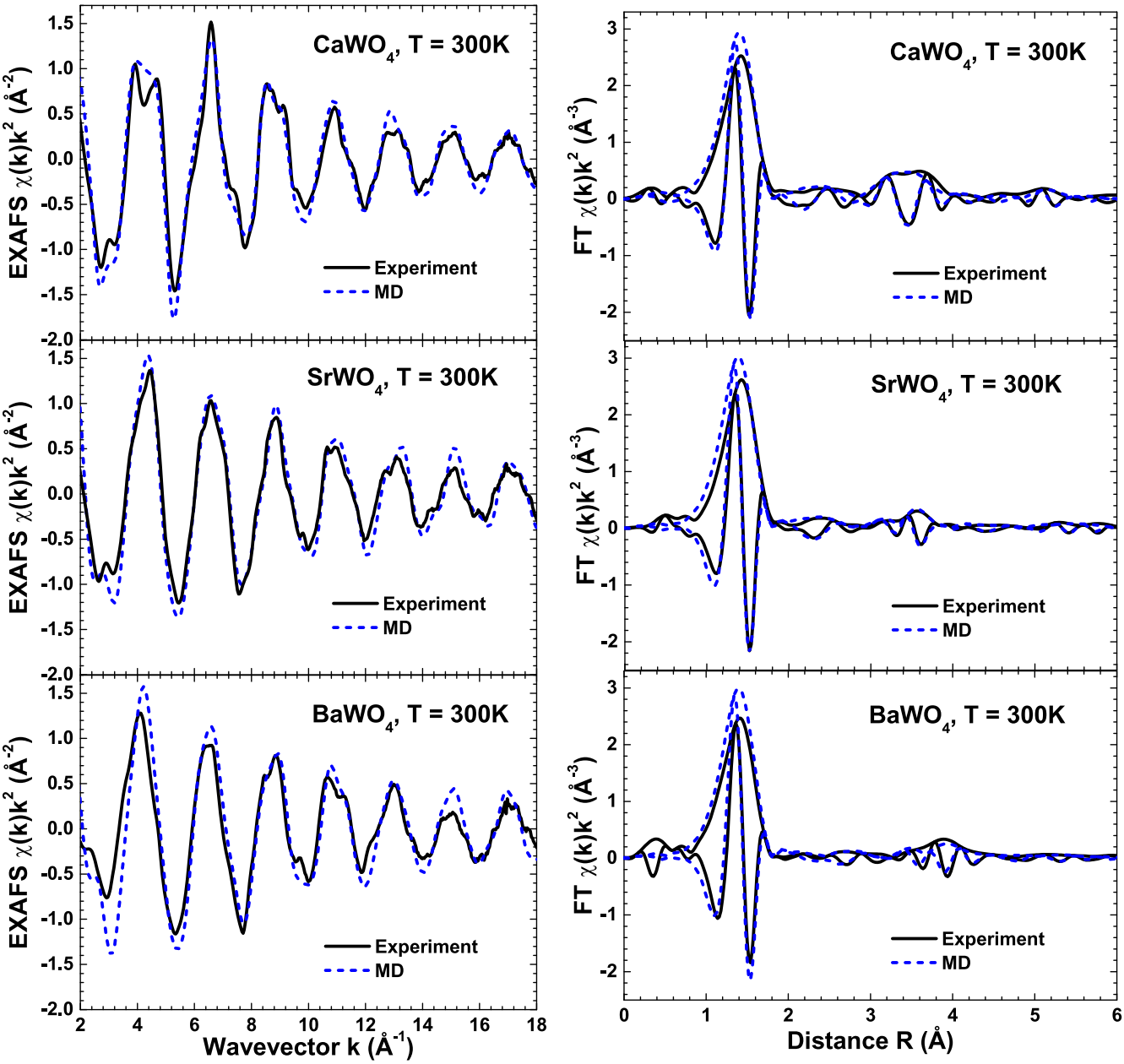

Figure 4. Comparison of the experimental and calculated by MD-EXAFS method W L_3-edge EXAFS $\chi(k)k^2$ spectra and their Fourier transforms (modulus and imaginary parts are shown) in scheelite-type AWO_4 (A = Ca, Sr, Ba) tungstates at $T = 300$ K.

mean square displacements (MSDs) for oxygen and tungsten atoms and the mean square relative displacements (MSRD) for the nearest W–O atom pairs (table 2). The obtained RDFs were also decomposed into a set of Gaussian functions to evaluate the coordination numbers, interatomic distances and MSRD values for the first five coordination shells of tungsten (table 3).

The EXAFS spectra for each atomic configuration were calculated by the *ab initio* real-space MS FEFF8.2 code [6]. The scattering potential and partial phase shifts were calculated only once for the cluster with the radius of 8 Å, centered at the absorbing tungsten atom, employing the complex exchange-correlation Hedin–Lundqvist potential and 15%-overlapped muffin-tin radii [4]. Thus, small variation of the cluster potential due to atom thermal motion was neglected. At the same time, the scattering amplitude and phase shift functions were recalculated for each scattering path, thus taking into account the variation of the path geometry during the MD simulation. The MS contributions up to the 6th order were taken into account. The parameter $S_0^2 = 1$ was used in all simulations.

The calculated configuration-averaged EXAFS spectra $\chi(k)k^2$ are compared with the experimental data in k- and R-spaces in figure 4.

4. RMC simulations

The W L_3-edge EXAFS spectra of tungstates were also modeled using RMC method based on EA implemented in the EvAX code [21, 23].

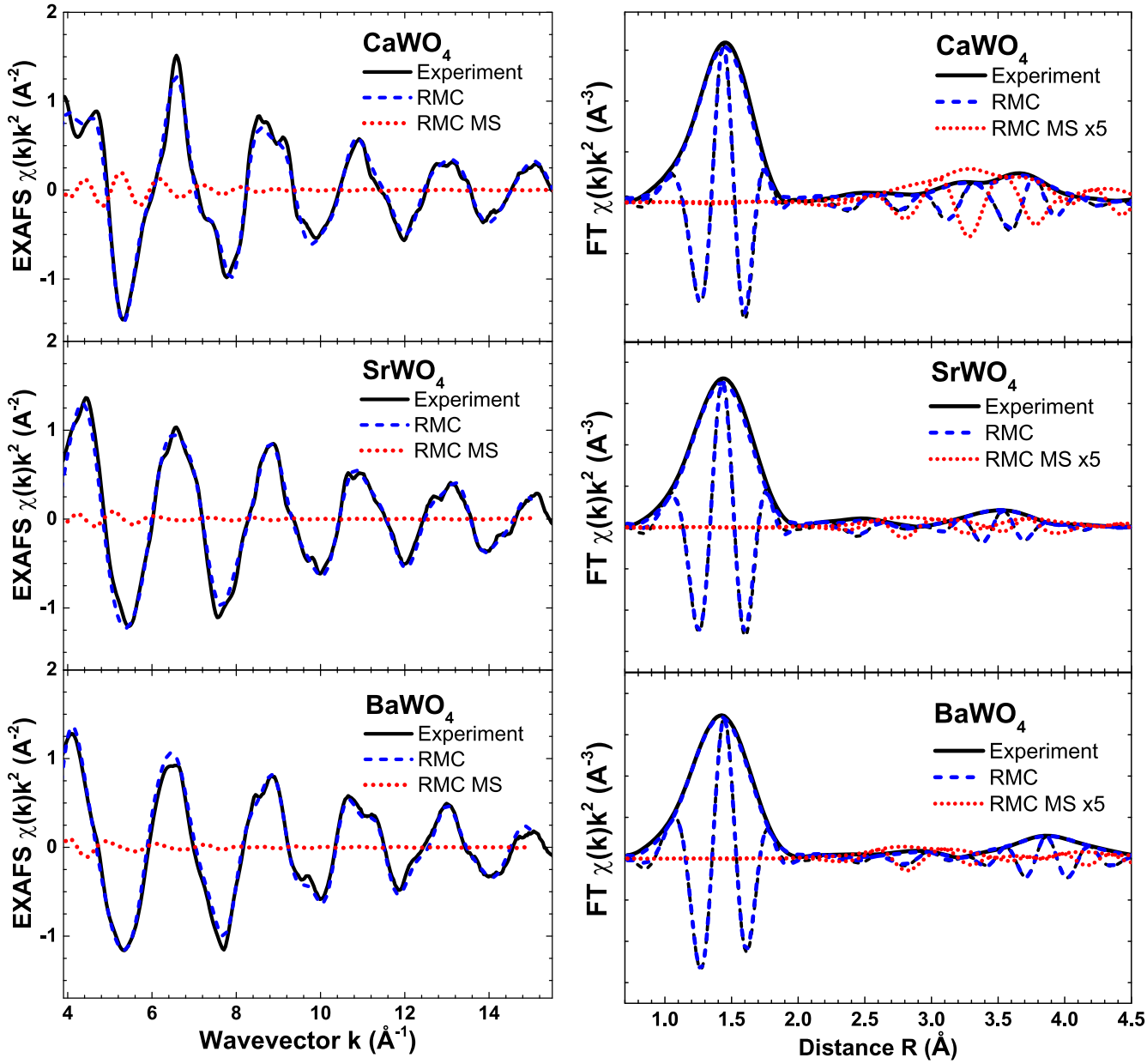

Figure 5. Comparison of the experimental (solid lines) and calculated by RMC/EA method (dashed lines) W L_3-edge EXAFS $\chi(k)k^2$ spectra and their Fourier transforms (modulus and imaginary parts are shown) in scheelite-type AWO_4 (A = Ca, Sr, Ba) tungstates at $T = 300$ K. The multiple-scattering contributions into the total calculated EXAFS spectra and their FTs are shown by dotted lines.

The simulation box was constructed as a supercell of $7a \times 7b \times 5c$ size with periodic boundary conditions. The equilibrium tungstate structure from diffraction experiments [30, 31] was used as initial structure model. RMC/EA calculations were simultaneously performed for 64 atomic configurations. A new atomic configuration was generated by randomly moving all atoms in the supercell within allowed maximal displacement of 0.4 Å.

The configuration-averaged EXAFS spectrum was calculated at each RMC/EA simulation step using the *ab initio* real-space MS FEFF8.50L code [6] with the same set of parameters as described in section 3. The comparison between theoretical and experimental EXAFS spectra $\chi(k)k^2$ was performed in k (from 4 to 15 $Å^{-1}$) and R (from 0.5 to 4.5 Å) spaces simultaneously using the Morlet wavelet transform (WT) [22].

The final configuration-averaged W L_3-edge EXAFS spectra $\chi(k)k^2$ and their FTs for three tungstates are compared with the experimental data in figure 5: the observed agreement is very good in k and R spaces. The contributions from the MS effects are separately shown in figure 5 by dotted line.

The atomic configurations, obtained as a result of RMC/EA simulations, were used further to calculate partial RDFs (figure 3) and MSRD(W–O1) parameters (table 2). Besides, the RDFs were decomposed into a set of Gaussian functions to calculate the coordination numbers, interatomic distances and MSRD values for the first five coordination shells of tungsten (table 3).

Due to a lack of sufficiently good statistics required for evaluation of the MSD parameters for W and O atoms

(table 2), they were estimated from MSRD values for W–W and O–O atomic pairs belonging to the same coordination shell at large (8–10 Å) distances, where a correlation of the atomic motion is negligible [46–48].

5. Results and discussion

The experimental W L_3-edge EXAFS spectra of AWO_4 (A = Ca, Sr, Ba) tungstates are shown in figure 2. Note that they have high signal-to-noise ratio in the full *k*-range. The three EXAFS spectra are rather similar due to the fact that the main contribution originates from the first coordination shell WO_4 tetrahedron with very close R(W–O) ≈ 1.78 Å distances (table 2). In fact, the first main peak in the FTs at 1.4 Å coincides in three compounds. However, the high frequency parts of the EXAFS differ significantly due to slightly different lattice parameters of tungstates (table 2) as well as the type of the A^{2+} cations. This difference is well observed in FTs at long distances ($R > \sim 3$ Å).

The results of the MD-EXAFS simulations for three tungstates are compared with the experimental W L_3-edge EXAFS data in figure 4. The observed agreement is relatively good, except for the first peak in FT at 1.4 Å: its amplitude is slightly larger in the calculated EXAFS due to underestimated values of the MSRD(W–O) factor. Nevertheless, the peaks due to outer coordination shells and the MS contributions are well reproduced up to 6 Å. This fact demonstrates the reliability of the force-field models used.

To understand the origin of the discrepancy for the first peak in FT at 1.4 Å, we performed lattice dynamics (LD) calculations in the harmonic approximation [40] using the same force-field models as in the MD simulations. As a result, the temperature dependence of the $MSRD_{LD}$(W–O) was calculated from the eigenvalues and eigenvectors of the dynamic matrix through the integral over all normal modes [49]. At $T = 0$ K the MSRD(W–O) values are solely due to the zero-point vibration and are equal to $MSRD_{LD} \sim 0.0012$ Å^2 for three tungstates, whereas their values at $T = 300$ K are twice larger ($MSRD_{LD} \sim 0.0024$ Å^2). Thus, our theoretical estimate suggests that quantum effects, which are neglected in our classical MD simulations, are important for the W–O bonding even at room temperature and constitute about 80% of the MSRD values. This result correlates well with the high values (~910–925 cm^{-1} at $T = 10$ K) of the W–O stretching frequencies in AWO_4 (A = Ca, Sr, Ba) tungstates found by Raman spectroscopy in [50].

In figure 5 we show the results of the RMC/EA simulations. Note that opposite to the MD-EXAFS case, where atomic coordinates were obtained directly from the MD runs, in the RMC method, which do not rely on any force-field model, the positions of all atoms are optimized to best fit the experimental EXAFS spectrum. Therefore, the obtained agreement between theory and experiment is much better, and all peaks in FTs are well reproduced. Note also that the disorder present in the atomic configurations obtained by the RMC method can be of static and dynamic origin, including quantum effects. Therefore, the RMC results should be compared with those from the lattice dynamics calculations. As one can see, the values of the RMC MSRD factors for the nearest W–O bonds at $T = 300$ K reported in table 2 are about twice smaller than $MSRD_{LD} \sim 0.0024$ Å^2. This indicates the need for further improvement of the force-field models of tungstates.

The MS contributions to the total calculated EXAFS spectra and their FTs are shown in figure 5 by dotted lines. Note that the amplitude of the FT modulus and imaginary parts were multiplied by a factor of five for better visibility. Comparing the MS contributions in three tungstates one can conclude that they are rather small but important at low *k*-values, and their amplitude decreases slightly from $CaWO_4$ to $BaWO_4$.

Structural results obtained by the MD and RMC methods can be compared using the partial radial distribution functions in figure 3 and a set of structural parameters (table 3) derived from a decomposition of the RDFs into Gaussian functions. Here the difference in the amplitude of the first peak at ~1.78 Å reflects the difference in the values of the MSRD (W–O) factors mentioned above. All other peaks up to 8 Å correspond to the respective coordination shells in the tungstate structure, and their position and amplitudes are close in the RDFs obtained by both methods. However, the RDFs obtained by RMC/EA method are slightly more broadened.

In spite of a similarity of crystal structures, the difference between three tungstates is well observed in the peak at ~4 Å of the RDFs $G(R)$ for the W–A atom pairs: the peak broadens going from $CaWO_4$ to $SrWO_4$ and splits into two parts in $BaWO_4$ (figure 3). This peak is due to two nearest groups of four A-type atoms in each, located in *ab*-plane and along the *c*-axis. The difference between the distances R(W–A) for two groups of atoms is equal to 0.16 Å in $CaWO_4$, 0.20 Å in $SrWO_4$, and 0.27 Å in $BaWO_4$, according to diffraction [30, 31]. The splitting have to be equal to zero in the ideal case ($c = 2a$) and reflects crystalline anisotropy of tungstates, appearing also in their anisotropic compressibility [51, 52] and thermal expansion [31, 53, 54]. The two groups of the W–A distances in $BaWO_4$ are resolved in both MD and RMC RDFs (figure 3) and are separated by 0.27 Å and 0.31 Å (table 3), respectively: these values are close to the diffraction data [30]. However, in the case of $CaWO_4$ and $SrWO_4$ the two groups of distances are not resolved in RMC RDFs, but still can be distinguished in the MD simulations, when *a priori* information to which group each atom belongs is available.

Finally, we would like to discuss isotropic amplitudes of thermal vibrations for W and O atoms reported in table 2. The experimental values of the MSD(O) and MSD(W) factors for three tungstates obtained from diffraction studies [30, 31] are rather close and do not show any clear dependence on the A-type cation. Note that the determination of MSD factors is a delicate task, and some spread of MSD values is observed in two experimental works [30, 31] for $CaWO_4$. The results of MD and RMC/EA simulations indicate an increase of both MSD factors going from $CaWO_4$ to $BaWO_4$, which can be explained by a significant increase of the unit-cell volume from 305.5 Å^3 for $CaWO_4$ to 350.7 Å^3 for $SrWO_4$ and,

finally, to 400.8 $Å^3$ for $BaWO_4$. Note that absolute values of the calculated MSD factors are close to the experimental values. The difference between a sum of the MSD factors for two atoms (i and j) and the MSRD for the atomic pair (i–j) provides information on the displacement correlation function (DCF) [55] and allows one to estimate a dimensionless correlation parameter ϕ [47, 56]

$$\phi = \frac{\mathrm{MSD}_i + \mathrm{MSD}_j - \mathrm{MSRD}_{ij}}{2\sqrt{\mathrm{MSD}_i}\sqrt{\mathrm{MSD}_j}}. \quad (1)$$

It is equal to +1 for perfectly in-phase atom motion, to zero for completely independent motion, and to −1 for perfectly antiphase motion. Using the values of MSD and MSRD factors from table 2, one can obtain the value of $\phi \approx 0.98$, i.e., the atomic motion of W and O atoms in three tungstates is strongly correlated. This indicates on strong covalent W–O bonding in WO_4 tetrahedra in agreement with the high frequency (908 cm^{-1} for $CaWO_4$, 918 cm^{-1} for $SrWO_4$, 922 cm^{-1} for $BaWO_4$ at $T = 300$ K) of the W–O stretching mode in Raman scattering spectra of tungstates [50]. Note that the value of ϕ in scheelites is only slightly larger than in a series of crystals with the diamond-zincblende structure as Ge, GaAs, InP, CdTe and CuCl, where it varies from 0.76 to 0.82 [57], and is close to the value in metal oxides as Cu_2O and Ag_2O, where $\phi \approx 0.97$ [57]. It was argued in [57] that the first-shell correlation along the interatomic bond is smaller for close-packed structures but increases upon decreasing of the coordination number. At the same time, the negligible dependence of ϕ on the degree of ionicity was found for the diamond–zinc–blende structure [57].

6. Conclusions

The room-temperature W L_3-edge EXAFS spectra of scheelite-type AWO_4 (A = Ca, Sr, Ba) tungstates were modeled using classical MD and RMC methods, taking into account MS contributions and thermal disorder effects.

The MD simulations, performed using the force-field models from [41, 42], underestimate the MSRD values for the nearest W–O atom pairs due to the neglect of quantum effects (table 2). At the same time, the RMC/EA simulations, which do not rely on any force-field model and are in a good agreement with the EXAFS data, suggest about 43% larger MSRD(W–O) values.

Despite that the EXAFS signal beyond the first coordination shell is weak, both MD and RMC/EA methods were able to describe correctly the changes in the tungstate structure and dynamics due to the presence of different alkaline Earth metal atoms. The obtained structural models were used to calculate partial RDF functions and to estimate MSD and MSRD parameters for tungsten and oxygen atoms. The increase of the splitting of the A-type atom group at ~4 Å from tungsten, reflecting the anisotropy of the tungstate structure, was clearly detected in both MD and RMC/EA simulations going from $CaWO_4$ to $BaWO_4$. We also found that the values of the MSD(O) and MSD(W) factors grow upon an increase of the unit cell volume, and the motion of tugsten and oxygen atoms is strongly correlated, so that the MSRD(W–O) factors remain small and close in three tungstates.

To conclude we have shown that the advanced analysis of EXAFS data based on MD and RMC/EA simulations provides useful information on crystal lattice structure and dynamics in tungstates.

Acknowledgments

The authors acknowledge the financial support of BMBF funding: SusChem (FKZ 05K13UK1) and Latvian Government Research grant no. 187/2012. The experiments at DESY have received funding from the European Community's Seventh Framework Programme (FP7/20072013) under Grant agreement no. 226716.

References

[1] Yano J and Yachandra V K 2009 *Photosynth. Res.* **102** 241–54
[2] Bordiga S, Groppo E, Agostini G, van Bokhoven J A and Lamberti C 2013 *Chem. Rev.* **113** 1736–850
[3] Kuzmin A and Chaboy J 2014 *IUCrJ.* **1** 571–89
[4] Rehr J J and Albers R C 2000 *Rev. Mod. Phys.* **72** 621–54
[5] Filipponi A, Di Cicco A and Natoli C R 1995 *Phys. Rev.* B **52** 15122
[6] Ankudinov A L, Ravel B, Rehr J J and Conradson S D 1998 *Phys. Rev.* B **58** 7565–76
[7] Rehr J J, Kas J J, Vila F D, Prange M P and Jorissen K 2010 *Phys. Chem. Chem. Phys.* **12** 5503–13
[8] Filipponi A and Di Cicco A 1995 *Phys. Rev.* B **52** 15135–49
[9] Gurman S J, Binsted N and Ross I 1984 *J. Phys. C: Solid State Phys.* **17** 143–51
[10] Tomić S, Searle B, Wander A, Harrison N, Dent A, Mosselmans J and Inglesfield J 2005 *New Tools for the Analysis of EXAFS: The DL EXCURV Package CCLRC Technical Report* DL-TR-2005-001 ISSN 1362-0207
[11] Palmer B J, Pfund D M and Fulton J L 1996 *J. Phys. Chem.* **100** 13393–8
[12] Okamoto Y 2004 *Nucl. Instrum. Methods Phys. Res.* A **526** 572–83
[13] Farges F, Lefrere Y, Rossano S, Berthereau A, Calas G and Brown G E Jr 2004 *J. Non-Cryst. Solids* **344** 176–88
[14] Ferlat G, Soetens J C, Miguel A S and Bopp P A 2005 *J. Phys.: Condens. Matter* **17** S145–57
[15] Kuzmin A and Evarestov R A 2009 *J. Phys.: Condens. Matter* **21** 055401
[16] Kalinko A, Evarestov R, Kuzmin A and Purans J 2009 *J. Phys.: Conf. Series* **190** 012080
[17] McGreevy R L and Pusztai L 1988 *Mol. Simul.* **1** 359–67
[18] Gurman S J and McGreevy R L 1990 *J. Phys.: Condens. Matter* **2** 9463–73
[19] Di Cicco A and Trapananti A 2005 *J. Phys.: Condens. Matter* **17** S135–44
[20] Brehm M and Kirchner B 2011 *J. Chem. Inf. Model.* **51** 2007–23
[21] Timoshenko J, Kuzmin A and Purans J 2014 *J. Phys.: Condens. Matter* **26** 055401
[22] Timoshenko J and Kuzmin A 2009 *Comp. Phys. Commun.* **180** 920–5

[23] Timoshenko J, Kuzmin A and Purans J 2012 *Comput. Phys. Commun.* **183** 1237–45
[24] Sleight A W 1972 *Acta Crystallogr.* B **28** 2899–902
[25] Errandonea D and Manjón F J 2008 *Prog. Mater. Sci.* **53** 711–73
[26] Timoshenko J, Anspoks A, Kalinko A and Kuzmin A 2014 *Phys. Scr.* **89** 044006
[27] Timoshenko J, Anspoks A, Kalinko A and Kuzmin A 2015 *Phys. Status Solidi* A **212** 265–73
[28] Timoshenko J, Anspoks A, Kalinko A and Kuzmin A 2015 *Z. Phys. Chem.* **230** 551–68
[29] Timoshenko J, Anspoks A, Kalinko A, Jonane I and Kuzmin A 2015 *Ferroelectrics* **483** 68–74
[30] Gürmen E, Daniels E and King J S 1971 *J. Chem. Phys.* **55** 1093–7
[31] Senyshyn A, Hoelzel M, Hansen T, Vasylechko L, Mikhailik V, Kraus H and Ehrenberg H 2011 *J. Appl. Crystallogr.* **44** 319–26
[32] Balerna A, Bernieri E, Burattini E, Kuzmin A, Lusis A, Purans J and Cikmach P 1991 *Nucl. Instrum. Methods Phys. Res.* A **308** 234–9
[33] Kuzmin A and Purans J 2001 *Radiat. Meas.* **33** 583–6
[34] Kuzmin A, Kalendarev R, Purans J, Itie J P, Baudelet F, Congeduti A and Munsch P 2005 *Phys. Scr.* **2005** 556–8
[35] Gracia L, Longo V M, Cavalcante L S, Beltran A, Avansi W, Li M S, Mastelaro V R, Varela J A, Longo E and Andres J 2011 *J. Appl. Phys.* **110** 043501
[36] Rickers K, Drube W, Schulte-Schrepping H, Welter E, Brüggmann U, Herrmann M, Heuer J and Schulz-Ritter H 2007 *AIP Conf. Proc.* **882** 905–7
[37] Aksenov V L, Kovalchuk M V, Kuzmin A Y, Purans Y and Tyutyunnikov S I 2006 *Crystallogr. Rep.* **51** 908–35
[38] Kuzmin A 1995 *Physica* B **208-209** 175–6
[39] Gale J D 1996 *Phil. Mag.* B **73** 3–19
[40] Gale J D and Rohl A L 2003 *Mol. Simul.* **29** 291–341
[41] Kalinko A and Kuzmin A 2013 *J. Phys.: Conf. Series* **430** 012075
[42] Senyshyn A, Kraus H, Mikhailik V B and Yakovyna V 2004 *Phys. Rev.* B **70** 214306
[43] Hoover W G 1985 *Phys. Rev.* A **31** 1695–7
[44] Hockney R W 1970 *Methods Comput. Phys.* **9** 136–211
[45] Kuzmin A, Anspoks A, Kalinko A and Timoshenko J 2016 *Z. Phys. Chem.* **230** 537–49
[46] Sapelkin A V and Bayliss S C 2002 *Phys. Rev.* B **65** 172104
[47] Jeong I K, Heffner R H, Graf M J and Bilinge S J L 2003 *Phys. Rev.* B **67** 104301
[48] Jonane I, Lazdins K, Timoshenko J, Kuzmin A, Purans J, Vladimirov P, Gräning T and Hoffmann J 2016 *J. Synchrotron Radiat.* **23** 510–8
[49] Cope E R and Dove M T 2007 *J. Appl. Crystallogr.* **40** 589–94
[50] Desgreniers S, Jandl S and Carlone C 1984 *J. Phys. Chem. Solids* **45** 1105–9
[51] Hazen R M, Finger L W and Mariathasan J W E 1985 *J. Phys. Chem. Solids* **46** 253–63
[52] Rodríguez-Hernández P *et al* 2006 *J. Phys. Chem. Solids* **67** 2164–71
[53] Deshpande V T and Suryanarayana S V 1972 *J. Mater. Sci.* **7** 255–6
[54] Achary S, Patwe S, Mathews M and Tyagi A 2006 *J. Phys. Chem. Solids* **67** 774–81
[55] Beni G and Platzman P M 1976 *Phys. Rev.* B **14** 1514–8
[56] Booth C H, Bridges F, Bauer E D, Li G G, Boyce J B, Claeson T, Chu C W and Xiong Q 1995 *Phys. Rev.* B **52** R15745
[57] Fornasini P and Grisenti R 2015 *J. Synchrotron Radiat.* **22** 1242–57